Article

Interlayer Adhesion of Coating System in Analogue and Digital Printing Technologies Formed on Lightweight Honeycomb Furniture Panels

Maciej Tokarczyk [1,2], Barbara Lis [1,*] and Tomasz Krystofiak [1,*]

1 Department of Wood Science and Thermal Techniques, Faculty of Forestry and Wood Technology, Poznan University of Life Sciences, Wojska Polskiego 28, 60-627 Poznan, Poland; maciej.tokarczyk@up.poznan.pl
2 BORNE-FURNITURE Company, Złotego Smoka St. 23, 66-400 Gorzów Wielkopolski, Poland
* Correspondence: barbara.lis@up.poznan.pl (B.L.); tomasz.krystofiak@up.poznan.pl (T.K.)

Abstract: This article concerns research into the influence of the energy dose distributed by UV lamps on selected parameters of varnish coatings formed during the varnishing process of lightweight cellular panels. The lightweight cellular board used in the study was made according to an innovative solution. The surface finishing of the boards was carried out using the roller method in combination with digital and analogue printing under industrial conditions. Contact angle measurements of the obtained varnish coatings were carried out, from which the surface free energy was calculated. In addition, interlayer adhesion was assessed by pull-off tests. Irrespective of the radiation dose, higher contact angle values (54.3–89.9°) were recorded for the last two applied layers (base coat 2 and base coat 3) than for the other coatings (39.6–64.1°). For all systems tested, the γs^p component showed lower values (2.25–28.99 mJ/m²) than γs^d (28.66–32.80 mJ/m²). The adhesion test results ranged from 0.5 to 0.9 MPa, although with varying types of delamination. Based on the test results, the most favourable variants from the furniture manufacturer's point of view were selected that provided the desired level of adhesion, in which cohesive damage located within the substrate (A) predominated.

Keywords: surface; UV lacquer system; UV ink system; printing technology; adhesion

1. Introduction

In today's times, when aesthetics and personalization play a crucial role in attracting consumer attention, manufacturers employ various techniques to make their products stand out in the market [1,2]. One such technique is creating prints on furniture panels using either analogue or digital methods. These methods allow for the production of high-quality products with a unique appearance, enabling customization to meet customer expectations. The introduction of these technologies into production processes provides a competitive advantage and satisfies even the most sophisticated customer needs [3].

Integrating the roller coating of UV products with digital or analogue printing allows for the replacement of natural materials, such as solid wood and thin veneers [4,5]. Combining these technologies and appropriately selecting process parameters reduces production costs using cheaper alternative materials, increases process efficiency, and effectively reduces the energy consumption required for production processes. This innovative technology not only allows manufacturers to compete effectively in the market by offering high-quality products with a modern look but also contributes to sustainable development by reducing the negative impact on the natural environment [3,6–9].

Replacing traditional materials with cheaper alternatives sometimes requires a different approach in technological finishing operations with lacquer products. A special case is the lacquering of lightweight panels with reinforcing elements, which are prone to dents and damage during finishing processes. Such cases can occur during roller application,

which allows for the application of base layers serving as substrates for subsequent layers in analogue and digital printing technologies.

The appropriate selection of topcoat lacquer products and printing inks, as well as the correct execution of individual printing stages, determines the achievement of a wood grain pattern similar to the original while maintaining the appropriate durability of finishes [10]. These aspects are essential to achieving high aesthetic and decorative value. Both methods enable personalization and give products a unique character. This is extremely important in today's diverse and rapidly changing market. In this regard, especially digital printing, which allows for the production of short series, offers broad possibilities for projects based on individual customer requirements. This approach enriches the offerings of businesses [1].

Another factor influencing the success of companies is the continuous increase in production efficiency, which can be achieved by shortening the production time of furniture components. This can be accomplished by increasing printing speed, which requires optimizing technological processes, including the selection of lacquer products, application parameters, and curing. Inappropriate process parameters will lower the quality of finishes. At too high speeds, lacquer coatings may not achieve the proper adhesion strength necessary for durability. This can be countered by adjusting, among other things, the formulation of lacquer products, the thickness of the applied product, the radiation dose, the exposure time, the temperature and moisture of the environment, the distance of radiators, and the number and types of radiators [7,11]. By modifying the formulation, one can influence their physico-chemical properties, thus affecting the interaction of lacquer products with the substrate, or between individual layers, and the curing speed [6,12–15]. One of the important components is the type of photoinitiator, which must be matched to the wavelength of the UV radiation source [16]. Additionally, the applied products must have the appropriate temperature, viscosity, surface tension, wettability, and, therefore, spreadability [15,17]. In terms of process parameters, the UV radiation power delivered during the curing of UV materials has a key impact on adhesion strength. This applies to both classic mercury and gallium UV lamps, whose selection depends on the type of product (transparent or pigmented) and energy-efficient UV LED lamps. These radiators differ in the spectrum of emitted light [16,18–22]. This affects the mentioned power of the radiators, which consists of intensity (W/cm^2) and in turn translates into the energy density (J/cm^2) delivered to the process. Their values determine the course of the polymerization of lacquer products based on the mechanism of free-radical reactions. Intensity initiates polymerization, while density determines the amount of energy per given surface area at a specific time. By changing these indicators, one can regulate the curing process, thereby influencing the adhesive properties of coatings [9,12,18,23–25].

A special role in the coating formation process and their adhesion is attributed to wetting phenomena. These can be assessed by measuring the wetting angle using goniometers and, based on it, determining, using theoretical assumptions, the work of adhesion strength or surface free energy. These issues have been discussed in many publications [26–33]. One can also use the method of wetting the surface with test liquids of varying surface tensions. These can quickly assess the surface condition for the application of lacquer products. The surface energy of the substrate and the formed coatings will condition the transfer of lacquer products through rollers and adhesion [17]. The above methods allow for indirect inference about the possibility of wetting the substrate. Direct methods include cross-cut tests and pull-off tests. Pull-off methods provide results in numerical form, ensuring the study's objectivity. Additionally, the percentage of delamination in the coating system can be determined. The results of studies conducted using these methods depend on many factors that influence the substrate-wetting process [34–39]. In the literature, no research works dedicated to the adhesion strength of UV lacquer coatings formed on the surface of cellular panels in the printing process were encountered. Due to the lack of literature data, it was decided to conduct studies dedicated to analyzing the influence of the energy dose distributed by UV radiators on the adhesive properties of lacquer coatings formed in the

process of roller lacquering lightweight cellular panels with discretely arranged reinforcing elements in combination with digital and analogue printing in production conditions.

2. Materials and Methods

2.1. Substrate and Coating Products

This study used samples with a construction based on lightweight cellular boards with HDF external facings and a cellular core with reinforcing blocks measuring 100 cm × 60 cm (Figure 1). They were made according to an innovative solution for which a patent has been granted for the invention titled "Method for manufacturing a cellular plate and a cellular plate manufactured by this method" [40]. Currently, approval is being awaited for the next EU-scale patent for the invention titled "Method for manufacturing an ultra-light cellular board with blocks and an ultra-light cellular board with blocks" (PL443573).
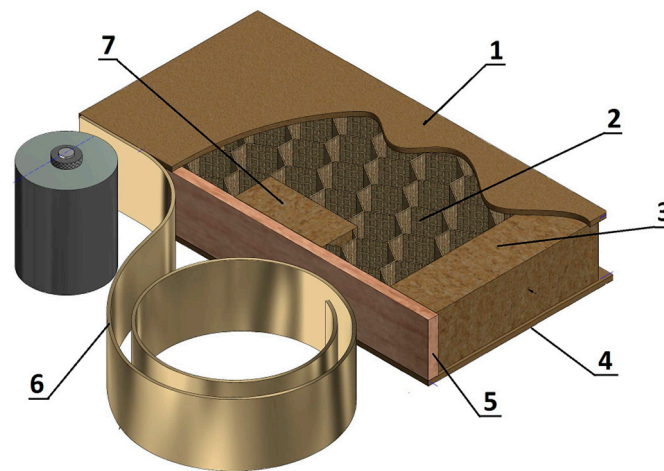

Figure 1. Lightweight wood-based honeycomb furniture panels with discreetly located strengthening blocks. Element descriptions: (1) top panel (HDF); (2) honeycomb; (3) cross bars (optional); (4) bottom panel (HDF); (5) support edge; (6) edge band (ABS); (7) strengthening blocks.

The application process of multi-layer coating systems with analogue printing was carried out at a line feed speed of 40 m/min according to the general concept presented in Figure 2.

Figure 2. Selected schematic diagram for refining the board furniture components with a roller method and analogue printing technology. Process description: (A1) sealer 1–30 g/m^2; (A2) sealer 2–20 g/m^2; (A3) basecoat –10 g/m^2; (A4) basecoat 1A–30 g/m^2; (A5) basecoat 2–25 g/m^2; (A6) topcoat 1–12 g/m^2; (S1,S2) sanding; (L1,L2,L3,L5) LED lamp 396 nm 12 W/cm^2; (SF1,SF2,SF3,SF4) super Focus Mercury Lamp 120 W/cm; (P1,P2,P3) analogue printers.

The line utilized offset machines (P1), (P2), and (P3) composed of a set of rollers. Using a rubber roller (the so-called offset cylinder), which picked up ink from the gravure roller, the image was transferred to the printed substrate.

Figure 3 presents the general concept of the application process of multi-layer coating systems with digital printing, which was also carried out at a line feed speed of 40 m/min.
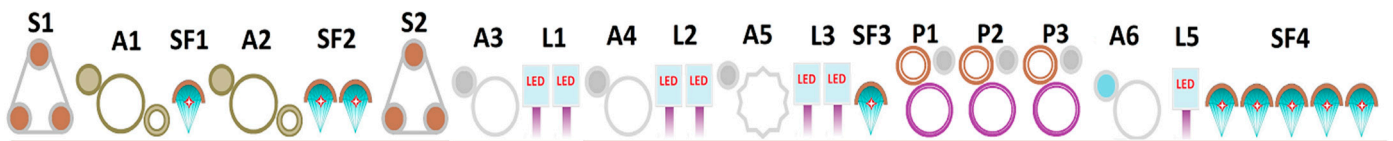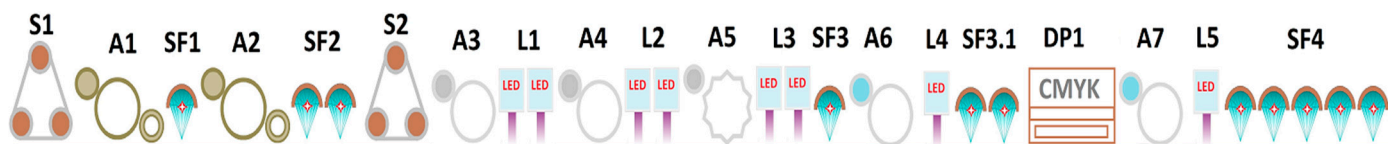
Figure 3. Selected schematic diagram for refining the board furniture components with a roller method and digital printing technology. Process description: (A1) sealer 1–30 g/m^2; (A2) sealer 2–20 g/m^2; (A3) basecoat–10 g/m^2 (A4) basecoat 1A–30 g/m^2 (A5) basecoat 2–25 g/m^2; (A6) topcoat 1–12 g/m^2; (A7) topcoat 2–6 g/m^2; (S1,S2) sanding; (L1,L2,L3,L4,L5) LED lamp 396 nm 12 W/cm^2; (SF1,SF2,SF3,SF3.1,SF4) Super Focus Mercury Lamp 120 W/cm; (DP1) CMYK digital printing machine.

The image creation process proceeded in CMYK mode (Cyan, Magenta, Yellow, Black), which involves applying the four primary colours in appropriate proportions to achieve a full range of colours (Figure 4). The image for printing was initially prepared in digital form. It was then transformed through RIP software (Raster Image Processor—Fiery XF Version 6.4) into four separate images representing each of the CMYK colours. The resulting images were defined in bitmap form (different shades represented as varying levels of colour saturation). These bitmaps were rasterized into a grid of small dots (pixels) adapted to the printer's resolution. Each dot was saved in raster format and corresponded to a specific colour saturation. Inks in CMYK colours were applied to the substrate through printing nozzles.
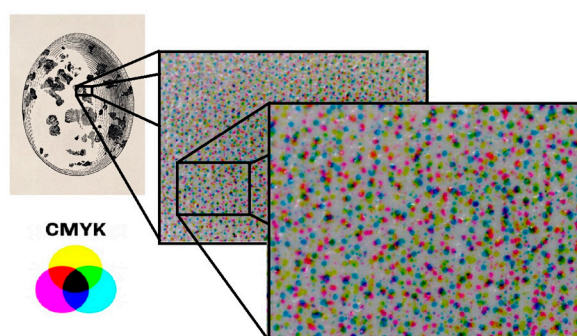
Figure 4. Grid of small CMYK dots (pixels) on a white substrate in digital printing technology (photo by Borne Furniture).

Table 1 shows the basic properties of UV varnish products based on the manufacturer's technical sheets.

Table 1. Properties of UV varnish products.

Properties	Name of UV Varnish Products				
	IQ-UV 03040 Sealer	IQ-UVC03284 Basecoat	IQ-UVC03285 Basecoat	Iq-Hyc02486 Ink	ANUVIA 1250 UV Ink
Polymer base Colour	acrylic colourless	acrylic white	acrylic white	waterborne black	acrylic CMYK
Solid content [%] Viscosity	95.3 ± 3 65–85 (flow cup 8 mm)	97.6 ± 3 90–140 (flow cup 6 mm)	97.5 ± 3 35–50 (flow cup 8 mm)	20 ± 3 20–35 (flow cup 4 mm)	15–25 (flow cup 4 mm)
Processing temperature [°C]	Between 20 and 50				

The templates prepared at different stages were transported to the laboratory, cut into samples, and left in an air-conditioned laboratory at 23 ± 2 °C, RH 50 ± 5%. A summary of the samples with the accepted labelling is given in Table 2.

Table 2. Preparation of the test substrate.

Samples	Speed [m/min]	Amount for Layer [g/m²]	Type	Energy UVA [mJ/cm²]	Energy UVV [mJ/cm²]	LED395 nm [mJ/cm²]
Process scheme (Stage I)						
3	40	50	sealer	114.8	111.9	-
4	40	50	sealer	89.0	85.6	-
5	40	50	sealer	57.4	55.9	-
6	40	50	sealer	26.2	26.1	-
Process scheme (Stage II)						
7	40	25	sealer	171.1	164.8	-
9	40	25	sealer	113.2	110.2	-
10	40	25	sealer	88.9	84.7	-
12	40	25	sealer	26.8	26.1	-
Process scheme (Stage III)						
27	40	12	base coat 1	-	-	443.9
29	40	12	base coat 1	-	-	346.0
30	40	12	base coat 1	-	-	288.5
32	40	12	base coat 1	-	-	196.1
Process scheme (Stage IV)						
27A	40	30	base coat 1A	-	-	443.9
29A	40	30	base coat 1A	-	-	346.0
30A	40	30	base coat 1A	-	-	288.5
32A	40	30	base coat 1A	-	-	196.1
Process scheme (Stage V)						
36	40	30	base coat 2	301.7	300.7	513.4
37	40	30	base coat 2	182.3	183.3	513.4
42	40	30	base coat 2	90.5	91.9	513.4
43	40	30	base coat 2	76.7	79.7	345.8
44	40	30	base coat 2	59.6	62.1	513.4
46	40	30	base coat 2	27.3	29.6	345.8
47	40	30	base coat 2	-	-	345.8

Table 2. *Cont.*

Samples	Speed [m/min]	Amount for Layer [g/m²]	Type	Energy UVA [mJ/cm²]	Energy UVV [mJ/cm²]	LED395 nm [mJ/cm²]
Process scheme (Stage VI)						
55	40	5	base coat 3	303.7	302.7	-
56	40	5	base coat 3	192.5	192.7	-
57	40	5	base coat 3	150.1	150.2	-
58	40	5	base coat 3	99.2	99.0	-
59	40	5	base coat 3	64.3	64.1	-
60	40	5	base coat 3	34.0	31.9	-
61	40	5	base coat 3	34.0	31.9	225.9

After 7 days of conditioning the samples, the visual assessment was carried out and the following measurements were taken: contact angle, surface energy and adhesion strength.

2.2. Research Method

2.2.1. Visual Assessment

Visual assessment was carried out with an unaided eye at a distance of 250 mm, incident at an acute angle to highlight the presence of potential surface defects.

2.2.2. Contact Angle

The contact angle measurement was conducted using an optical tensiometer, OneAttension Theta (Biolin Scientific AB, Gothenburg, Sweden). Distilled water was used as the wetting liquid. Water droplets of 3.5 µL volume were applied to the surface by "slowly depositing them onto the surface". The camera recorded its behaviour in contact with the substrate for 60 s. Based on the data obtained, specialized software analyzed the shape of the droplet by determining the value of the contact angle. Building upon the data of the contact angle obtained for a water droplet stabilized for 10 s and in compliance with the assumptions of the adsorption theory of adhesion, the interactions between the substrate and individual layers of the coating system of the values of surface free energy (γS), together with the dispersion and polar components, were determined.

2.2.3. Measurements of Surface Energy

Measurements of surface energy were conducted using coloured test inks based on ethanol/water with varying surface tensions.

- Series 24, 26 28, 30, 32, 34, 36, 38, 40, 42, 44, 46, 48, 50, 54, 58, 62, 66, and 72 mN/m.

For each tested sample, ink was applied as a strip using a brush at 3 different locations. When the surface of the test liquid remained smooth without showing any tendency to separate on the paint coatings, it was assumed that the surface tension level corresponded to the value indicated on the respective bottle.

2.2.4. Adhesion Strength of Coatings

The test was carried out in compliance with EN ISO 4624. The surfaces of the specimens were notched using a hob cutter and then 20 mm diameter measuring stamps were glued using silane/epoxy adhesive. After a conditioning period of 168 h, stamps were then peeled off with an automated driven Positest AT-A test device (DeFelsko Corporation, Ogdensburg, NY, USA). Five tests were carried out on each test system with the layers (Figure 5). The images of delamination under destructive loadings were assessed visually, taking into account the rating scale in Table 3.
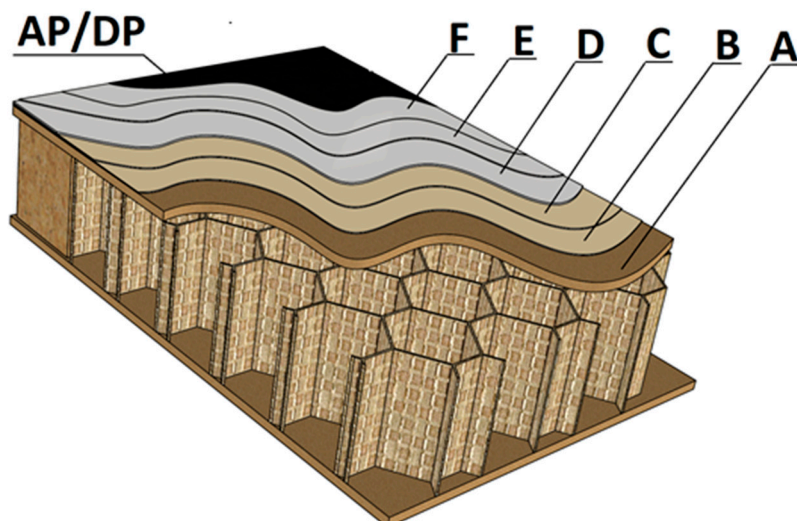
Figure 5. Sample with labelled layers.

Table 3. Measurement system's parameters.

Detachment Type	Detachment Occurring in a Given System
A	Cohesive in a substrate
A/B	Adhesive between a substrate and the first sealer
B	Cohesive in the first sealer
B/C	Adhesive between the first sealer and second sealer
C	Cohesive in the second sealer
C/D	Adhesive between the second sealer and first base coat
D	Cohesive in the first base coat
D/E	Adhesive between the first base coat and second base coat
E	Cohesive in the second base coat
E/F	Adhesive between the second base coat and third base coat
F	Cohesive in the third base coat
E/AP or DP	Adhesive between the second base coat and printings
F/AP or DP	Adhesive between the second base coat and printings
AP	Cohesive in the analogue printings
DP	Cohesive in the digital printings

3. Results

The prepared samples were characterized by a high quality. No defects were observed on the surface of the coatings, indicating that the substrate finishing stages were carried out correctly. In addition, no defects were observed after their transport to the testing laboratory, which confirms its adequate delivery conditions and control over the mode of transport. When assessing the appearance of the surface, an increase in the homogeneity of the varnish coating was observed in the function of the applied coatings.

3.1. Visual Assessment

During the evaluation of the appearance of the prepared paint finishes under varying energy doses distributed by UV radiators, no adhesion issues were observed. Both the adhesion strength between the substrate and the primer layer and between the individual layers formed using printing technology showed no signs of delamination during organoleptic assessment. This indicates that all actions taken during the production process were executed correctly. The aesthetics of the various options were also acceptable, with no defects noticed on the surfaces except for samples 36 and 55, where greater granularity was noted due to the excessive curing of the coating. This resulted in the reduced flowability of the applied product, leading to uneven distribution on the surface. Other differences

in the quality of the formed coatings only became apparent during surface property tests, including measurements of the contact angle, surface energy, and adhesion strength.

3.2. Contact Angle

The average contact angle values are provided in Table 4.

Table 4. Formation of the contact angle at various stages of the process.

Marking of Samples	Speed [m/min]	Amount for Last Layer [g/m^2]	Kind of Lacquer Product	Mean of Contact Angle [degrees]	Max.	Min.	Standard Deviation	Coefficient of Variation [%]
3	40	50	sealer	60.8	63.3	57.5	2.4	3.87
4	40	50	sealer	57.8	58.5	56.1	1.0	1.76
5	40	50	sealer	51.1	53.3	49.7	1.4	2.65
6	40	50	sealer	43.8	45.1	41.7	1.3	2.90
7	40	25	sealer 2	64.1	66.7	61.7	1.9	2.89
9	40	25	sealer 2	62.7	65.4	58.5	2.8	4.53
10	40	25	sealer 2	61.6	63.8	59.8	2.0	3.23
12	40	25	sealer 2	57.7	59.7	55.5	1.6	2.72
27	40	12	base coat 1	55.1	56.2	53.7	1.1	1.97
29	40	12	base coat 1	51.4	53.1	49.9	1.2	2.40
30	40	12	base coat 1	48.7	50.1	47.7	0.9	1.85
32	40	12	base coat 1	45.2	46.7	42.8	1.7	3.81
27A	40	30	base coat 1A	51.9	53.5	49.7	1.5	2.82
29A	40	30	base coat 1A	45.2	46.4	44.0	0.9	1.96
30A	40	30	base coat 1A	42.5	45.1	40.4	1.9	4.57
32A	40	30	base coat 1A	39.6	42.6	37.7	1.8	4.59
36	40	30	base coat 2	89.9	92.3	87.7	1.7	1.85
37	40	30	base coat 2	83.3	84.8	81.0	1.6	1.91
42	40	30	base coat 2	77.0	79.0	75.3	1.4	1.77
43	40	30	base coat 2	75.3	76.4	73.8	0.9	1.26
44	40	30	base coat 2	71.4	73.4	69.8	1.3	1.84
46	40	30	base coat 2	61.3	63.5	58.8	1.9	3.07
47	40	30	base coat 2	54.3	55.9	52.2	1.4	2.56
55	40	5	base coat 3	84.1	86.4	81.6	1.7	2.05
56	40	5	base coat 3	82.4	83.3	80.8	1.0	1.20
57	40	5	base coat 3	80.4	82.2	78.7	1.3	1.63
58	40	5	base coat 3	77.5	78.5	76.0	1.1	1.38
59	40	5	base coat 3	75.3	77.8	72.1	2.2	2.92
60	40	5	base coat 3	65.3	67.0	63.8	1.2	1.78
61	40	5	base coat 3	66.8	68.2	65.6	1.0	1.55

Based on the obtained results, it is worth emphasizing that the collected measurement data demonstrated very high repeatability, as evidenced by the statistical parameters, with a coefficient of variation below 5%. By evaluating these relationships in the process of analogue and digital printouts, it was found that the surface-wetting process is influenced by the energy density of the radiation. At all stages of coating formation, it was observed that with a decrease in the UV radiation dose, the contact angle value decreased. This correlation occurs regardless of the type of lamp used for the polymerization process, leading to the hardening of the lacquer products. Moreover, it was observed that the tested lacquer systems, after exposure to mercury lamps emitting a spectrum with different wavelengths (from UV-C to the infrared range), exhibited a higher contact angle (65.3° up to 84.1°) than those cured with a monochromatic UV LED light spectrum (39.6° up to 55.1°). This indicates different degrees of coating cross-linking, caused by the different spectral characteristics of the lamps. The degree of polymerization could also have been

influenced by the varied UV radiation absorption by the lacquer products, resulting from their different formulations and properties.

In addition to its cross-linking effect, UV radiation can cause side effects such as shrinkage processes and the resulting stresses in the lacquer coatings, or changes in bond lengths. This can lead to surface variations, manifesting as irregularities or porosity in the coatings [41–45]. Structural changes in the lacquer layers may also be affected by the degree of photoinitiator migration [42]. Furthermore, there is a correlation between substrate interaction and coating roughness [46–48]. The application of successive layers alters the topography of the previously applied coating. The issue of wettability in relation to roughness has been addressed in many scientific studies [34,49–57]. In the present research, the base layers generally exhibited lower values of this parameter compared to the top layers, regardless of the radiation dose. This correlation could also be influenced by the aforementioned coating topography, which is also confirmed by the authors' previous work on the adhesion of coatings in analogue and digital printing [48]. This promotes interaction between the applied lacquer and the substrate or subsequent coatings. It is assumed that lacquer products better wet the surfaces, which in turn facilitates the formation of interlayer adhesive bonds [48,58,59].

Generally, for base layers (sealer and sealer 2; base coat 1 and base coat 1A), lower values of this parameter were recorded (39.6–64.1) compared to base coat 2 and base coat 3 (54.3–89.9), regardless of the radiation dose. This is a beneficial phenomenon in the function of the number of layers applied in the printing process, promoting interaction between the applied lacquer and the substrate or subsequent coatings. It is assumed that lacquer products better wet the surfaces, which simultaneously promotes the formation of interlayer adhesive bonds [41–43]. The evaluation of the results also showed that the thickness of the finish, which increased during the printing process, did not explicitly affect the contact angle value. With each subsequent layer, a change in this parameter was recorded; however, no increase was obtained with the increase in radiation energy density at all stages of printouts. After applying the second filler (Stage II), smaller changes in the contact angle were observed (Figure 6).
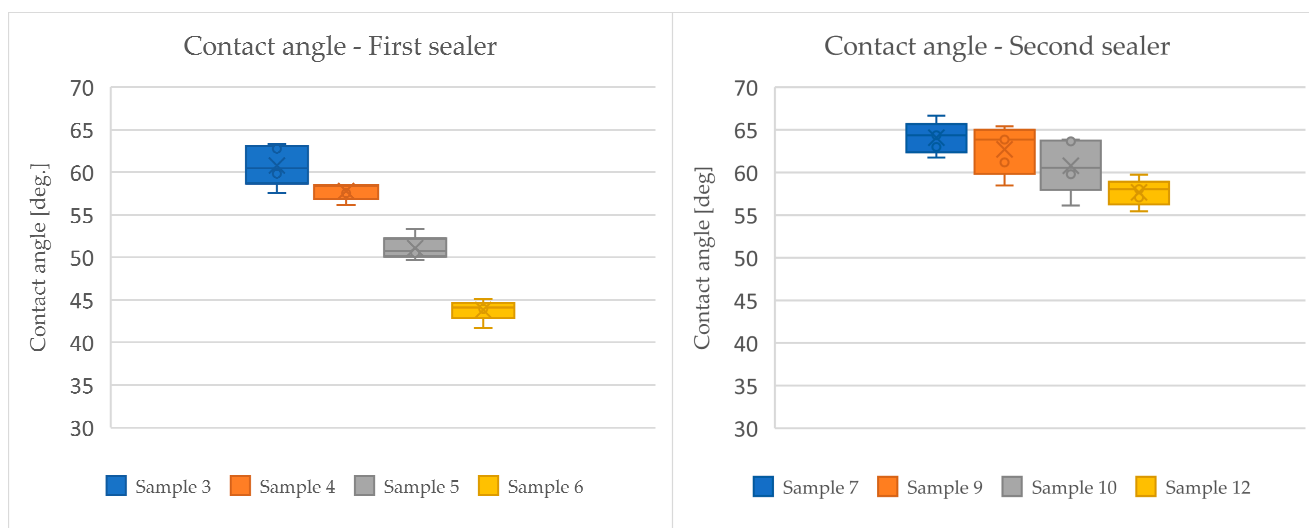

Figure 6. Formation of the contact angle after applying the sealers.

In the subsequent stages (III and IV), the contact angle decreased (Figure 7).

The formed layers, regardless of the energy dose delivered by the 395 nm LED emitters (Figure 7), were less cross-linked compared to the use of mercury lamps. As previously mentioned, this is a beneficial phenomenon from the perspective of the wetting process by subsequent layers and the formation of adhesive bonds. In the final phase of the process, where a lacquer layer was applied for printing, significant changes in the contact angle

were observed for both layers cured using the combined technique (LED + mercury lamps) and those cured solely with mercury lamps (Figure 8). This process was carried out at a temperature of 30 ± 5 °C and relative humidity of 40 ± 10%. The distance between the LED radiators and the substrate was fixed at 20 mm.

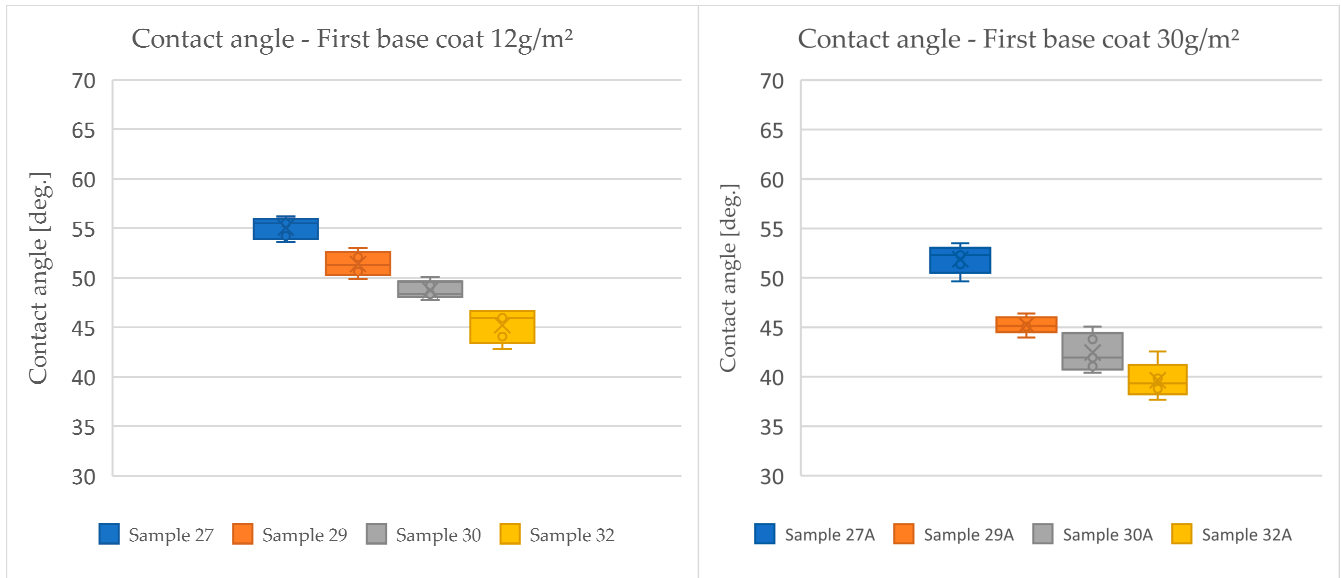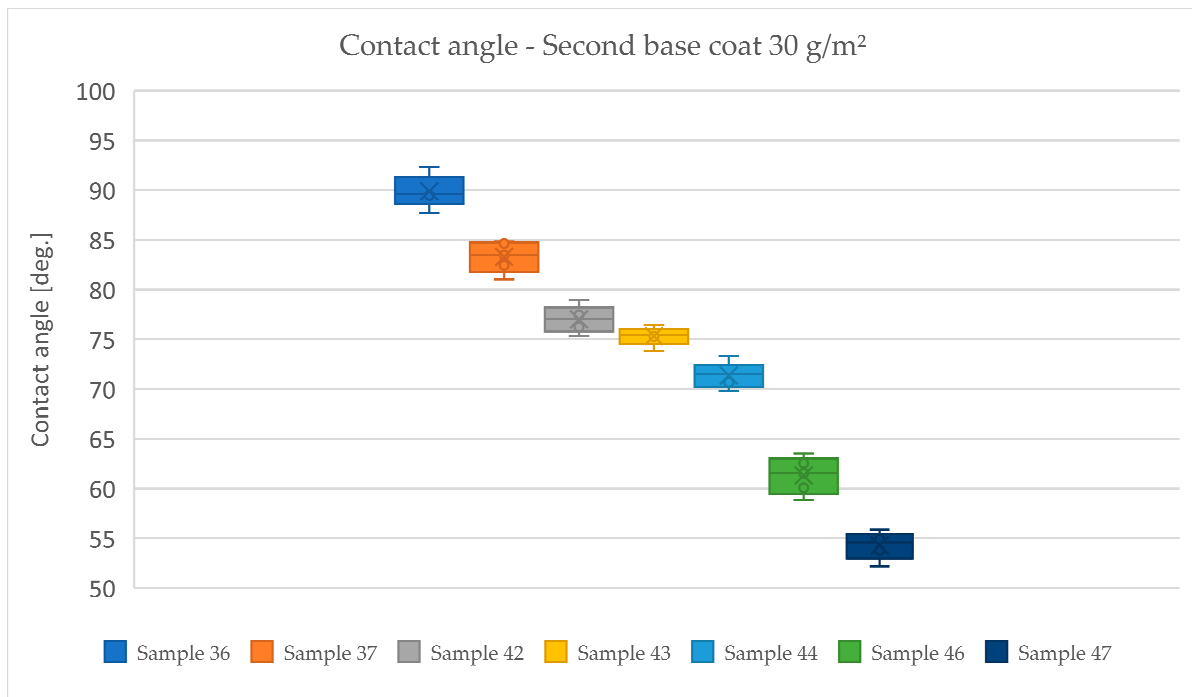**Figure 7.** Formation of the contact angle after applying base coatings.

Figure 8. Formation of the contact angle after applying the layer for analogue and digital printing (Stage V).

Especially at the highest energy doses distributed by the emitters, a significant increase in this parameter was observed with respect to the base layers (Figure 9). This is a highly beneficial phenomenon from the perspective of the performance characteristics of the final products. In summary, for the radiation doses used in the study, the contact angle was highest (89.9°) at maximum doses for both LED and mercury emitters (UVA 301.7 mJ/m^2; UVV 300.7 mJ/m^2; LED395 nm 513.4 mJ/m^2). This suggests that the degree of cross-linking

of the coatings formed at these doses is the greatest. As the radiation dose decreased, the degree of polymerization also decreased, and the surfaces were not fully cured.
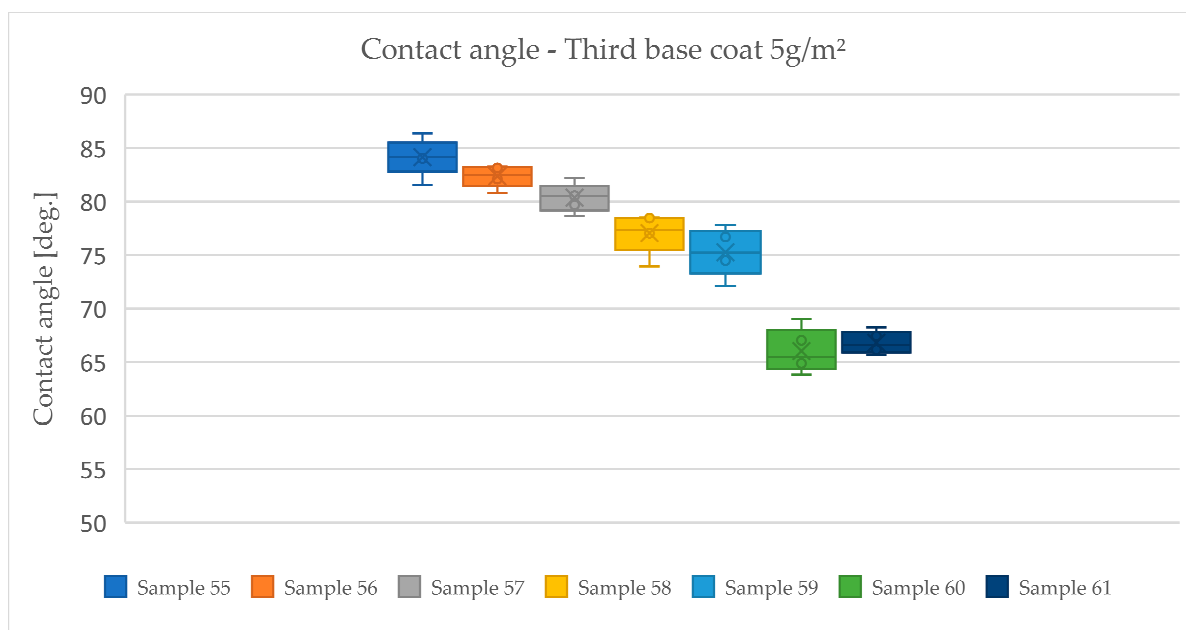

Figure 9. Formation of the contact angle after applying the layer for analogue and digital printing (Stage VI).

3.3. Measurements of Surface Energy

Table 5 presents the values of γs for the coatings, along with their dispersive and polar components.

Analyzing the γs values for the various stages of the printing process, a clear influence of the radiation dose on the resulting surface free energy could be observed. As the contact angle of the analyzed coatings decreased, an increasing trend in this parameter was noted. The highest surface free energy 59.28 mJ/m^2 was exhibited by sample 32A, cured with an LED emitter at the lowest energy dose LED395 nm 196.1 mJ/cm^2 in Stage IV of the printing process. In contrast, sample 36, after applying the final layer of lacquer and exposing it to the highest radiation dose from a mercury lamp (UVA 301.7 mJ/m^2; UVV 300.7 mJ/m^2; LED395 nm 513.4 mJ/cm^2), exhibited the lowest γs value (30.91 mJ/m^2). Analyzing the relationships regarding the components of surface free energy, it can be noted that γsp showed significantly lower values compared (2.25–28.99 mJ/m^2) to γsd for all studied systems. The γsd values of the coatings were relatively consistent (28.66–32.80 mJ/m^2). Greater variation was observed for γs^p. Given this, the γs values of the individual coatings were primarily determined by γsp.

The results demonstrating the impact of the radiation dose on surface properties and the quality of decorative finishes were confirmed by direct adhesion tests using the pull-off method.

Measurements of Surface Energy by Ink Stripes

The obtained results of the surface energy state for the various variants are summarized in Table 6. An example is presented in Figure 10, showing a sample with the arrangement of ink stripes under different tensions.

Table 5. Result of surface free energy γS, along with its components (dispersive γS^d and polar γS^p), for coatings formed during the printing process.

| Samples	Speed [m/min]	Amount for Last Layer [g/m²]	Type	γ_s	γ_s^d	γ_s^p
				[mJ/m²]		
3	40	50	sealer	46.96	32.79	14.17
4	40	50	sealer	48.72	32.70	16.02
5	40	50	sealer	52.67	32.16	20.51
6	40	50	sealer	56.91	31.09	25.82
7	40	25	sealer 2	45.02	32.78	12.25
9	40	25	sealer 2	45.84	32.80	13.05
10	40	25	sealer 2	46.37	32.80	13.57
12	40	25	sealer 2	48.78	32.70	16.08
27	40	12	base coat 1	50.32	32.54	17.78
29	40	12	base coat 1	52.50	32.20	20.30
30	40	12	base coat 1	54.08	31.86	22.22
32	40	12	base coat 1	56.11	31.33	24.78
27A	40	30	base coat 1A	52.20	32.25	19.95
29A	40	30	base coat 1A	56.11	31.33	24.78
30A	40	30	base coat 1A	57.65	30.86	26.80
32A	40	30	base coat 1A	59.28	30.29	28.99
36	40	30	base coat 2	30.91	28.66	2.25
37	40	30	base coat 2	34.17	30.26	3.90
42	40	30	base coat 2	37.56	31.51	6.05
43	40	30	base coat 2	38.50	31.78	6.72
44	40	30	base coat 2	40.92	32.32	8.60
46	40	30	base coat 2	46.66	32.80	13.87
47	40	30	base coat 2	50.67	32.49	18.18
55	40	5	base coat 3	33.85	30.13	3.72
56	40	5	base coat 3	34.75	30.51	4.24
57	40	5	base coat 3	35.82	30.92	4.89
58	40	5	base coat 3	37.28	31.42	5.86
59	40	5	base coat 3	38.61	31.81	6.81
60	40	5	base coat 3	44.21	32.73	11.48
61	40	5	base coat 3	43.45	32.67	10.78
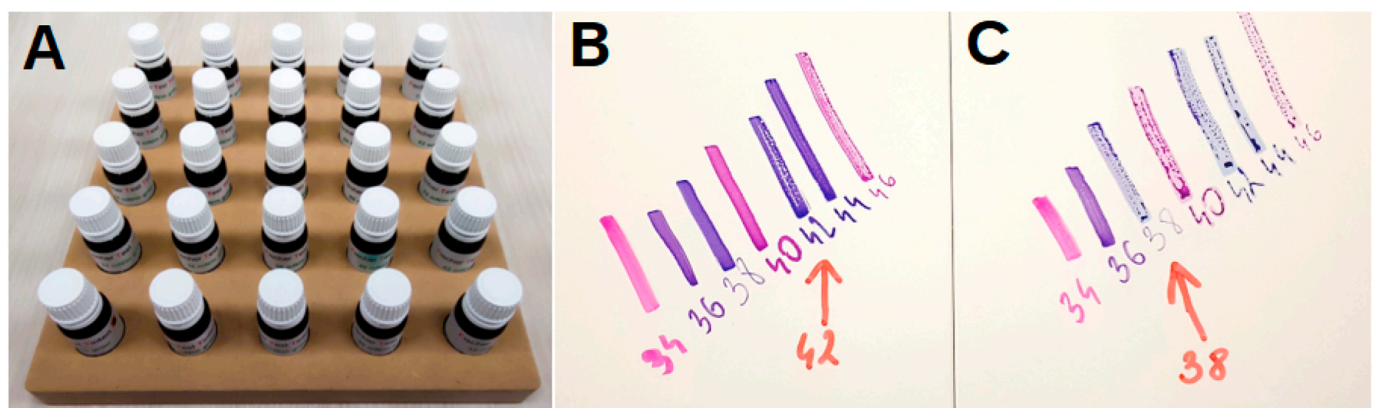
Figure 10. Variants with applied ink stripes of specific surface tension. (**A**) Full set of inks used for the studies; (**B**) result reading for values 42 mN/m; (**C**) result reading for values 38 mN/m.

Analyzing the obtained data, it is possible to observe varying surface properties of the individual coatings. The excessive cross-linking of the surface (free energy below 35 mJ/m^2) leads to adhesion problems between the substrate and the print. In the first four stages of the printing process, all systems exhibited the formation of a continuous ink band without separation into droplets, ranging from 42 mJ/m^2 to 48 mJ/m^2. Exceptions were variants 30, 32, and 32A, which achieved values of 52–54 mJ/m^2. In the subsequent stages, which involved applying the layer for printing, this parameter showed greater variation. The highest (54 mJ/m^2) and comparable levels (50–54 mJ/m^2) were demonstrated by variants 30, 32, 32A, 46, 60, and 61. For the third layer, the highest value > 55 mJ/m^2 was recorded for system 47. The lowest ink tension range of 28–30 mJ/m^2 was observed for sample 36. Overall, this test confirmed certain dependencies of the radiation dose on the development of surface energy. The test can be used for a rough assessment.

Table 6. Results of surface energy measurements for the individual variants.

Samples	Speed [m/min]	Amount for Last Layer [g/m^2]	Type	Evaluation of Test Inks [mJ/m^2]
3	40	50	sealer	42–44
4	40	50	sealer	42–44
5	40	50	sealer	52–54
6	40	50	sealer	52–54
7	40	25	sealer 2	42–44
9	40	25	sealer 2	42–44
10	40	25	sealer 2	42–44
12	40	25	sealer 2	42–44
27	40	12	base coat 1	46–48
29	40	12	base coat 1	46–48
30	40	12	base coat 1	52–54
32	40	12	base coat 1	52–54
27A	40	30	base coat 1A	46–48
29A	40	30	base coat 1A	46–48
30A	40	30	base coat 1A	46–48
32A	40	30	base coat 1A	52–54
36	40	30	base coat 2	28–30
37	40	30	base coat 2	30–32
42	40	30	base coat 2	36–38
43	40	30	base coat 2	36–38
44	40	30	base coat 2	46–48
46	40	30	base coat 2	52–54
47	40	30	base coat 2	56–58
55	40	5	base coat 3	28–30
56	40	5	base coat 3	30–32
57	40	5	base coat 3	38–40
58	40	5	base coat 3	38–40
59	40	5	base coat 3	38–40
60	40	5	base coat 3	50–52
61	40	5	base coat 3	50–52

3.4. Adhesion Strength

In Table 7, the adhesion strength results are summarized, while the types of delamination are provided in Table 3.

Table 7. Type of delamination occurring in the tested variants after adhesion strength test.

Samples	Speed [m/min]	Amount for Last Layer [g/m^2]	Type	Evaluation of Adhesion				
3	40	50	sealer	100A	100A	100A	100A	100A
4	40	50	sealer	80A, 20A/B	100A	100A	100A	80A, 20A/B
5	40	50	sealer	60A, 40A/B	25A, 75A/B	40A, 60A/B	60A, 40A/B	40A, 60A/B
6	40	50	sealer	80A, 20A/B	70A, 30A/B	30A, 70A/B	40A, 60A/B	20A, 80A/B
7	40	25	sealer 2	100A	100A	100A	100A	100A
9	40	25	sealer 2	100A	100A	100A	95A, 5A/B	90A, 5B, 5A/B
10	40	25	sealer 2	80A, 20C	85A, 15C	90A, 10C	85A, 15C	85A, 15C
12	40	25	sealer 2	70A, 30C	85A, 5C, 10B/C	85A, 10C, 5B/C	70A, 30C	95A, 5B/C
27	40	12	base coat 1	100A	90A, 10A/B	100A	70A, 30A/B	100A
29	40	12	base coat 1	70A, 30A/B	50A, 50A/B	100A	90A, 10A/B	100A
30	40	12	base coat 1	20A, 80C/D	100C/D	15A, 85C/D	15A, 85C/D	25A, 75C/D
32	40	12	base coat 1	100C/D	100C/D	100C/D	100C/D	100C/D
27A	40	30	base coat 1A	100A	100A, 10A/B	100A	70A, 30A/B	80A, 20A/B
29A	40	30	base coat 1A	70A, 30A/B	30A, 70A/B	100A/B	100A/B	100A/B
30A	40	30	base coat 1A	100C/D	100A/B	15A, 85C/D	15A, 85C/D	25A, 75D
32A	40	30	base coat 1A	100C/D	100C/D	100C/D	100C/D	100C/D
				Last layers with analogue printings				
36	40	30	base coat 2	100E/AP	100E/AP	100E/AP	100E/AP	100E/AP
37	40	30	base coat 2	100E/AP	100E/AP	10A, 90E/AP	20A80E/AP	100E/AP
42	40	30	base coat 2	70A, 30E/AP	100A	90A, 10A/B	100A	100A
43	40	30	base coat 2	70F, 20A, A/B	70A, 30A/B	100E	100F	5A, 95E
44	40	30	base coat 2	100D/E	20A, 80E	10A, 90D/E	100D/E	100D/E
46	40	30	base coat 2	100D/E	100D/E	100D/E	100D/E	90E, 10D/E
47	40	30	base coat 2	100D/E	100D/E	100D/E	100D/E	100D/E
55	40	5	base coat 3	100F/AP	10A, 90F/AP	100F/AP	100F/AP	100F/AP
56	40	5	base coat 3	100A	95A, 5B/C	100F/AP	95A, 5A/B	100A
57	40	5	base coat 3	100A	95A, 5B/C	100A	100A	100A
58	40	5	base coat 3	100A	95A, 5B/C	100A	95A, 5B/C	100A
59	40	5	base coat 3	100A	90A, 10A/B	80A, 20A/B	100A	100A
60	40	5	base coat 3	75A, 25A/B	100A	100A	95A, 5A/B	100A
61	40	5	base coat 3	80A, 20A/B	75A, 25A/B	80A, 20A/B	80A, 20A/B	75A, 25A/B
				Last layers with digital printings				
36	40	30	base coat 2	100E/DP	10A, 90E/DP	100E/DP	100E/DP	100E/DP
37	40	30	base coat 2	25A, 75	90E/DP	75A, 25E	90E/10DP	10A, 90E/DP
42	40	30	base coat 2	30A, 75A/B	100A	100A	90A, 10A/B	100A
43	40	30	base coat 2	5A, 95EE	5A, 95EE	20A, 80A/B	5A, 95E	100E
44	40	30	base coat 2	100D/E	20A, 80E	10A, 90D/E	100D/E	100D/E
46	40	30	base coat 2	100D/E	100D/E	100D/E	100D/E	90E, 10D/E
47	40	30	base coat 2	100D/E	100D/E	100D/E	100D/E	100D/E
55	40	5	base coat 3	10A, 90F/DP	10A, 90F/DP	10A, 90F/DP	30A, 70F/DP	100F/DP
56	40	5	base coat 3	100A	100B/C	95A, 5B/C	100B/C	100B/C
57	40	5	base coat 3	95B/C, 5C	95B/C, 5C	95B/C, 5C	95B/C, 5C	95B/C, 5C
58	40	5	base coat 3	95A, 5A/B	100A	95A, 5B/C	100A	100A
59	40	5	base coat 3	85A, 15A/B	100A	100A	85A, 15A/B	100A
60	40	5	base coat 3	45A, 55A/B	85A, 15A/B	85A, 15A/B	95A, 5A/B	95A, 5A/B
61	40	5	base coat 3	75A, 25A/B	95A, 5A/B	100A	100A	90A, 10A/B

The adhesion test results ranged from 0.5 to 0.9 MPa, although with varying types of delamination. The analysis of the obtained data indicates a clear influence of the radiation dose (min. UVA 26.2 mJ/cm^2 UVV 26.1 mJ/cm^2 up to max. UVA 301.7 mJ/m^2; UVV 300.7 mJ/m^2; LED395 nm 513.4 mJ/m^2) on the cross-linking and interlayer adhesion of the different systems. Based on the damaged images of the variants prepared in Stage I of the printing process, it was found that using a mercury radiation dose in the UVA range of 89–114 mJ/cm^2 and UVV range of 85–112 mJ/cm^2 ensured the complete cross-linking of the filler (systems 3 and 4). For these systems, 100% delamination occurred at the substrate (HDF board). This indicates that the weakest link in the adhesion tests of the coatings

was the HDF board. For variants with a double application of filler (Stage II), the best results (100% A) were recorded with the use of a mercury emitter in the UVA range of 112–172 mJ/cm^2 and UVV range of 110–165 mJ/cm^2. In contrast, energy densities below UVA 112 mJ/cm^2 and UVV 110 mJ/cm^2 were insufficient for complete cross-linking and maintaining 100% A adhesion. The analysis of interlayer adhesion after applying a single layer of base coating at 12 g/m^2 cured with LED lamps (Stage III) and a single layer of base coating at 30 g/m^2 cured with LED lamps (Stage IIIA) demonstrated favourable adhesion only when using an LED lamp with a power of 18 W/cm^2 delivering UVA 395 nm–346 mJ/cm^2. For Stage IV, the use of emitters with lower power than 18 W/cm^2 also led to insufficient cross-linking (mixed delamination mechanism with increasing prevalence of adhesive delamination between the first and second base coats 100C/D). A complete lack of adhesion was observed for the coating with an LED emitter power of 4 W/cm^2 (100E delamination—cohesive in the first base coat or second base coat).

When assessing the variants from stage V with a base coat layer for analogue and digital printing, which were cross-linked using a combined method (LED lamps + mercury lamps), full hardening (mostly 100% A) was found using the power of LED lamps of 24 W/cm^2, providing energy above UVV 395 nm–500 mJ/cm^2 and Hg 120 W/cm providing UVA 90 mJ/cm^2 and UVV 92 mJ/cm^2 (system 42), and in turn, a complete lack of adhesion was recorded for layers with analogue and digital printing in the case of variant 36 (no AP adhesion and DP). This indicates the excessive hardening of the coating (Figure 11).
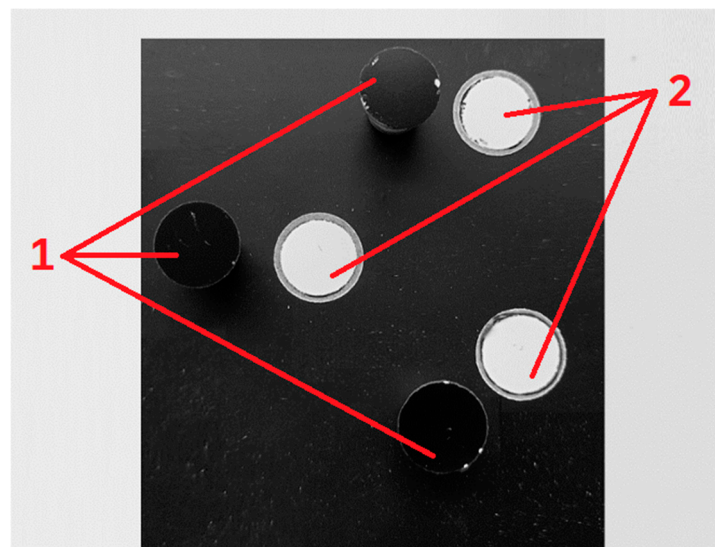

Figure 11. Adhesive delamination between base coat layers and printings. (1) Print layer visible on the stamp; (2) background layer for printing remaining on the sample.

Usage of mercury emitters with a power of <100 W/cm^2 proved insufficient (systems 43–47), as did reducing LED lamps to below 18 W/cm^2, delivering UVA 395 nm–346 mJ/cm^2 (Figure 12).

The analysis of the adhesion of the third thin layer (5 g/m^2) applied for digital and analogue printing (Stage VI—samples 55–61) demonstrated that adhesion was achieved for system 58 (using a 120 W/cm^2 Hg emitter) despite the absence of an LED lamp. System 55 showed no adhesion for both analogue and digital printing layers (no adhesion AP and DP). Additionally, system 56 exhibited no adhesion in the analogue printing range, indicating the excessive cross-linking of the coating. The use of a combined system (variant 61 with 12 W/cm^2 LED and 40 W/cm^2 Hg) yielded similar results, though with slightly lower delaminations at the substrate (80%A, 205A/B).
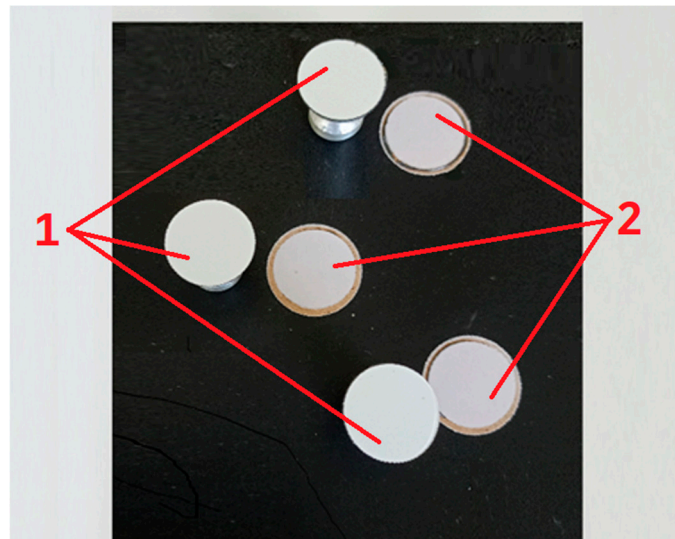
Figure 12. Adhesive delamination between first and second base coats (D/E). (1) Second base coat visible on the stamp; (2) first base coat remaining on the sample.

Combining systems 3 or 4 (stage I, stage II) with 7 or 9, followed by 27 (stage III, stage IV) and ultimately using systems 42 (stage V) or 58 (stage VI) for analogue and digital printing yields the best-quality results, ensuring the desired adhesion level of 100A. In these cases, the weakest link in the adhesion tests of the coatings was the substrate (Figure 13).
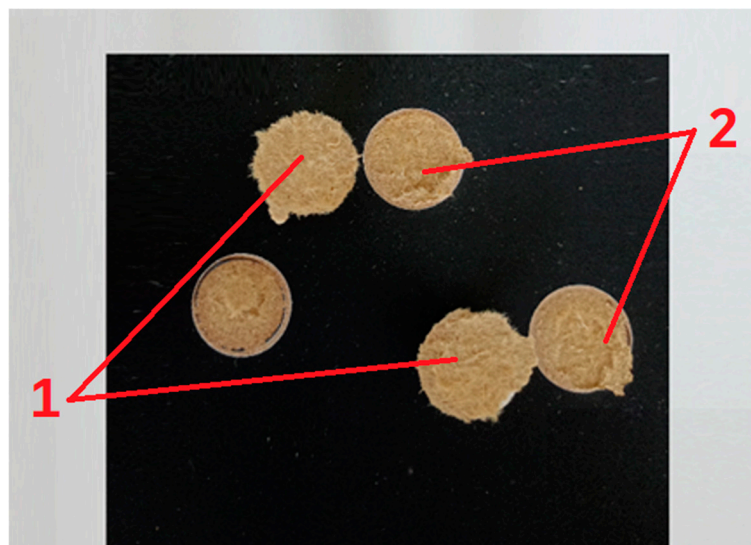
Figure 13. Cohesive delamination in substrate (expected result). (1) Inner layers of HDF board visible on the stamp; (2) inner layers of HDF board remaining on the sample.

4. Conclusions

In the surface interactions of cured systems in the substrate–printing relationship—in terms of the adhesion phenomenon—the following was found:

The excessive cross-linking of the surface (free energy below 35 mJ/m^2) leads to adhesion problems between the substrate and the print.

Mercury lamps most influence the formation of the wetting account.

For base layers (sealer and sealer 2; base coat 1 and base coat 1A), lower values of this parameter were recorded (39.6–64.1) compared to base coat 2 and base coat 3 (54.3–89.9), regardless of the radiation dose.

Based on the surface properties and adhesion tests carried out, the following were considered to be the best from a technological point of view, respectively:

Stage I: Samples 3 and 4. The first layer of sealer was applied directly onto the HDF board substrate. Both variants exhibit similarly acceptable properties as a base layer for the second layer of sealer (minimum recommended energy density: UVA 89.0 mJ/m^2; UVV 85.6 mJ/m^2).

Stage II: Samples 7 and 9. The second layer of sealer was applied onto the first sealer. Both variants exhibit similarly acceptable properties as a base layer for the first base coat (minimum recommended energy density: UVA 113.2 mJ/m^2; UVV 110.2 mJ/m^2).

Stage III: Sample 27. The first layer builds a colour by first applying a 12 g/m^2 coloured base coat (recommended energy density: LED395 nm 346.0 mJ/cm^2).

Stage IV: Sample 27A. The first layer builds a colour by first applying a 30 g/m^2 coloured base coat. This is preferred for cases requiring an intense colour coverage, hardened with an energy density of LED395 nm > 346.0 mJ/cm^2.

Stage V: Sample 42 (for analogue and digital printing). The second base coat consists of 30 g/m^2. It can be used as a background for analogue and digital printing technologies. For the curing process, the use of both types of emitters is necessary (UVA 90.5 mJ/m^2; UVV 91.9 mJ/m^2; LED395 nm 513.4 mJ/m^2).

Stage VI: Sample 58. The third base coat is created by applying 5 g/m^2. This layer is preferred as the optimal background for digital printing due to greater control over surface free energy. For the curing process, only a mercury lamp is sufficient (UVA 99.2 mJ/m^2; UVV 99.0 mJ/m^2). Regarding adhesion for digital printing, layouts 56 and 57 also scored well; however, there were problems with their print quality (graininess).

The results obtained regarding interlayer adhesion (adhesion of individual layers) give favourable indications for applications in industrial settings and demonstrate the need for work on selecting the number and power of innovative LEDs.

An inadequate choice of parameters can lead to the inadequate cross-linking of the applied layers and, as a result, to insufficient adhesion, which is decisive for the attractiveness, usability, and durability of the finishes.

The marker test confirmed some correlations between radiation dose and changes in surface free energy. This test can be used for preliminary assessment.

The developed printing technology on wood-based substrates represents an innovative solution that enhances consumer satisfaction not only in terms of product properties, such as adhesion, but also in aesthetics and unique designs. This technology positively impacts process stability and reproducibility, reducing costs associated with poor quality and minimizing production waste. Additionally, it aligns well with sustainable development policies by utilizing recycled materials, such as honeycomb panels and thin HDF substrates, and by reducing energy consumption through the use of LED radiators.

References

1. Pawlak, D.; Boruszewski, P. Digital printing in wood industry. *Ann. WULS For. Wood Technol.* **2020**, *109*, 109–115. [CrossRef]
2. Hagedorn, L.; Kremer, G.; Stark, R. Strengthening Aesthetic Individualization in Product Design to Enhance Customer Loyalty and Sustainability. In *EcoDesign and Sustainability II*; Springer: Berlin/Heidelberg, Germany, 2020.
3. Altun, S.; Köse, D. Some of the Physical Properties of UV Jet Printed Furniture Surfaces. *Drv. Ind.* **2013**, *64*, 39–43. [CrossRef]
4. Feng, X.; Wu, Z.; Ruijuan, S.; Fei, W.; Yayuan, Z.; Meijin, W. Surface Design of Wood-Based Board to Imitate Wood Texture Using 3D Printing Technology. *Bioresources* **2019**, *14*, 8196–8211. [CrossRef]
5. Sang, R.; Manley, A.; Wu, Z.; Feng, X. Digital 3D Wood Texture: UV-Curable Inkjet Printing on Board Surface. *Coatings* **2020**, *10*, 1144. [CrossRef]
6. Mendes, C.; Oliveira, J.; Etxebarria, I.; Vilas, J. Lanceros-Méndez, S. State-of-the-Art and Future Challenges of UV Curable Polymer-Based Smart Materials for Printing Technologies. *Adv. Mater. Technol.* **2019**, *4*, 1800618. [CrossRef]
7. Angelski, D. Influences of some factors upon the accelerated curing of pigmented polyurethane gloss top-coat by UV irradiation. In Proceedings of the 9th Hardwood Conference, Sopron, Hungary, 30 April 2020; pp. 7–12.
8. El-Rahman, A.; Saad, E.A.; Aydemir, C.; Özsoy, A.S.; Yenidoğan, S. Drying methods of the printing inks. *J. Graph. Eng. Des.* **2021**, *12*, 29–37. [CrossRef]
9. Patil, R.S.; Thomas, J.; Patil, M.; John, J. To Shed Light on the UV Curable Coating Technology: Current State of the Art and Perspectives. *J. Compos. Sci.* **2023**, *7*, 513. [CrossRef]
10. Proszyk, S. *Technologia Tworzyw Drzewnych cz. 2. Wykończanie Powierzchni*; WsiP: Warszawa, Poland, 1999; pp. 1–374.
11. Jašúrek, B.; Vališ, J.; Hozmanová, M. Influence of printing speed and radiation dose on the curing of UV inks and varnishes. In Proceedings of the 9th International Symposium on Graphic Engineering and Design, Novi Sad, Serbia, 8–10 November 2018; pp. 333–339. [CrossRef]
12. Stowe, R.W. Comparing Traditional UV Systems with LED UV Systems for UV Curing. In Proceedings of the AIMCAL Web Coating & Handling Conference USA the Association of International Metallizers, Coaters & Laminators, Myrtle Beach, SC, USA, 20–22 October 2014.
13. Khadzhynova, S.; Jakucewicz, S. *Sposoby Drukowania Cyfrowego*; Politechnika Łódzka: Łódź, Poland, 2016; pp. 1–242.
14. Ramirez, J.; Tumolva, T. Analysis and optimization of water-based printing ink formulations for polyethylene films. *Appl. Adhes. Sci.* **2018**, *6*, 1. [CrossRef]
15. Tomerlin, R.; Valdec, D.; Tomisa, M.; Vusic, D. The Impact of Underlying Opaque White Coating Parameters on Flexographic Print Quality. *Appl. Sci.* **2023**, *13*, 8575. [CrossRef]
16. UV-LED Curing—Eco-Friendly and Energy-Saving Technology. Available online: https://www.textiletechnology.net/technology/trendreports/STFI-UV-LED-curing-%E2%80%93-eco-friendly-and-energy-saving-technology-for-textile-industry-30338 (accessed on 31 May 2021).
17. Rentzhog, M. Characterisation of Water-Based Flexographic Inks and Their Interactions with Polymer-Coated Board. Master's Thesis, KTH Royal Institute of Technology, Stockholm, Sweden, 2004.
18. Lis, B.; Proszyk, S.; Krystofiak, T. Low energy consuming of hardening of lacquer coatings by means of UV–LED radiators. *Inthercathedra* **2009**, *25*, 75–79.
19. Borysiuk, P.; Derda, M.; Auriga, R.; Boruszewski, P.; Monder, S. Comparison of Selected Properties of Varnish Coatings Curing with the Use of UV and UV-LED Approach. *Ann. Wars. Univ. Life Sci.-SGGW For. Wood Technol.* **2015**, *92*, 49–54.
20. Landry, V.; Blanchet, P.; Boivin, G.; Bouffard, J.-F.; Vlad, M. UV-LED Curing Efficiency of Wood Coatings. *Coatings* **2015**, *5*, 1019–1033. [CrossRef]
21. Li, T.; Lin, F.; Ji, M.; Huang, B.; Cheng, W.; Shi, L.; Xia, M.; Wang, L. Development and Measurement of a 365 NM UV LED Irradiance Source. *Meas. Sens.* **2021**, *18*, 100153. [CrossRef]
22. Kraśkiewicz, A.; Kowalczyk, A. Radiation Curing of Phosphorus Telomer-Based Coatings Using UV LEDs or Medium-Pressure Mercury Lamp. *Materials* **2023**, *16*, 7493. [CrossRef]
23. Phoseon Technology, Peak Irradiance & Energy Density. A Phoseon Technology White Paper April 2018. Available online: https://www.google.com/url?sa=t&source=web&rct=j&opi=89978449&url=https://phoseon.com/wp-content/uploads/2019/03/Phoseon-White-Paper_April-2018_Power-vs-Irradiance.pdf&ved=2ahUKEwiptdaRwKSHAxUQQ_EDHVFoDmAQFnoECBcQAQ&usg=AOvVaw1PZuQcBMkCJ9I1B36F_835 (accessed on 29 June 2024).
24. Phoseon Technology, Dlaczego Całkowita Moc UV Jest Ważna dla Utwardzania UV LED? Świat DRUKU 9/2023, 28. Available online: https://www.google.com/url?sa=t&source=web&rct=j&opi=89978449&url=https://swiatdruku.eu/content/download/61232/614509/version/1/file/Dlaczego+ca%25C5%2582kowita+moc+UV+jest+wa%25C5%25BCna+dla+utwardzania+UV+LED.pdf&ved=2ahUKEwi0ysv-jaKHAxXoR_EDHa6aCokQFnoECBUQAQ&usg=AOvVaw1EzGGAtmMQiP4u6M_9zHzN (accessed on 20 May 2024).
25. Energy Density Matters . . . and This is Why. Available online: https://uvebtech.com/articles/2021/energy-density-mattersand-this-is-why/ (accessed on 20 May 2024).
26. Kloubek, J. Calculation of surface free energy components of ice according to its wettability by water, chlorbenzene and carbon disulfide. *J. Colloid Interface Sci.* **1974**, *46*, 185–190. [CrossRef]
27. Liptáková, E.; Kúdela, J. Analysis of the Wood-Wetting Process. *Holzforschung* **1994**, *48*, 139–144. [CrossRef]
28. Kúdela, J.; Liptáková, E. Adhesion of coating materials to wood. *J. Adhes. Sci. Technol.* **2006**, *20*, 875–895. [CrossRef]

29. Żenkiewicz, M. Methods for the calculation of surface free energy of solids. *J. Achiev. Mater. Manuf. Eng.* **2007**, *24*, 137–145.

30. Erbil, H. The debate on the dependence of apparent contact angles on drop contact area or three-phase contact line: A review. *Surf. Sci. Rep.* **2014**, *69*, 325–365. [CrossRef]

31. Palencia, M. Surface free energy of solids by contact angle measurements. *J. Sci. Technol. Appl.* **2017**, *2*, 84–93. [CrossRef]

32. Benkreif, R.; Brahmia, F.Z.; Csiha, C. Influence of moisture content on the contact angle and surface tension measured on birch wood surfaces. *Eur. J. Wood Prod.* **2021**, *79*, 907–913. [CrossRef]

33. Aydın, İ. Surface tension, contact angle and wettability of wood. *Wood Ind. Eng.* **2024**, *6*, 18–27.

34. Pecina, H.; Paprzycki, O. *Lack auf Holz*; Vincentz Verlag: Hannover, Germany, 1995; pp. 1–175.

35. Lis, B.; Krystofiak, T. Badania adhezji powłok lakierowych do drewna. Maksymalna przyczepność. In *Lakiernictwo Przem. Uszlachetnianie Powierzchni Drewna cz.2, Goldman*; Goldman: Tczew, Poland, 2010; pp. 44–46.

36. Sickfeld, J. Pull-Off Test, an Internationally Standardized Method for Adhesion Testing-Assessment of the Relevance of Test Results. In *Adhesion Aspects of Polymeric Coatings*; Mittal, K.L., Ed.; Springer: Boston, MA, USA, 1983; pp. 543–567. [CrossRef]

37. Maxwell, A.S. *Review of Test Methods for Coating Adhesion*. NPL Report No.: MATC(A)49. 2001, Volume 49, pp. 1–47. Available online: http://eprintspublications.npl.co.uk/id/eprint/2077 (accessed on 20 May 2024).

38. Dilik, T.; Erdinler, E.; Hazir, E.; Koc, K.; Hiziroglu, S. Adhesion Strength of Wood Based Composites Coated with Cellulosic and Polyurethane Paints. *Adv. Mater. Sci. Eng.* **2015**, *1*, 1–5. [CrossRef]

39. Łach, M.; Róg, G.; Ochman, K.; Pławecka, K.; Bąk, A.; Korniejenko, K. Assessment of Adhesion of Geopolymer and Varnished Coatings by the Pull-Off Method. *Eng* **2022**, *3*, 42–59. [CrossRef]

40. Tokarczyk, M. Layered Cellular Board. Patent Number PL435052A1, 28 February 2022.

41. Park, J.-W.; Shim, G.-S.; Lee, J.-G.; Jang, S.-W.; Kim, H.-J.; Choi, J.-N. Evaluation of UV Curing Properties of Mixture Systems with Differently Sized Monomers. *Materials* **2018**, *11*, 509. [CrossRef]

42. Nowakowski, P. Badania Migracji Wybranych Fotoinicjatorów (4-PBZ i TPO-L) z Pokrytych Poliakrylowymi Lakierami Opakowań Przeznaczonych do Kontaktu z Żywnością. Ph.D. Thesis, Uniwersytet Marii Curie-Skłodowskiej w Lublinie, Wydział Chemii Instytut Nauk Chemicznych, Lublin, Polska, 2020.

43. Tao, Y.; Sun, G.; Wei, Y.; Liu, R.; Zhao, J. An anti-shrinkage model of an ultraviolet-curing coating filled with hollow polyurethane acrylate microspheres. *Mech. Mater.* **2021**, *163*, 334–339. [CrossRef]

44. Zhang, H.; Feng, X.; Wu, Y.; Wu, Z. Effect of Photoinitiator Concentration and Film Thickness on the Properties of UV-Curable Self-Matting Coating for Wood-Based Panels. *Forests* **2023**, *14*, 1189. [CrossRef]

45. Moeck, A.; Bianchi, R.; Volker Petry, V.; Weder, R.; Helsby, D. Shrinkage of UV Oligomers and Monomers. Available online: https://www.google.com/url?sa=t&source=web&rct=j&opi=89978449&url=https://www.radtech.org/2014proceedings/papers/technical-conference/Formulation/Moeck%2520-%2520Shrinkage%2520of%2520UV%2520Oligomers%2520and%2520Monomers.pdf&ved=2ahUKEwja6ces2YGIAxUgLBAIHczuFnQQFnoECBwQAQ&usg=AOvVaw1DkP00RyOmmEFRH7GsohiA (accessed on 21 May 2024).

46. Bekhta, P.; Lis, B.; Krystofiak, T.; Bekhta, N. Surface Roughness of Varnished Wood Pre-Treated Using Sanding and Thermal Compression. *Forests* **2022**, *13*, 777. [CrossRef]

47. Slabejová, G.; Šmidriaková, M. The effect of coating film thickness on the quality of surface finish on lightweight plywood. *Acta Fac. Xylologiae Zvolen* **2022**, *64*, 39–58. [CrossRef]

48. Tokarczyk, M.; Lis, B.; Salca, E.A.; Krystofiak, T. Adhesion of Varnish Coatings as a Background for Analogue and Digital Printing Technologies. *Appl. Sci.* **2023**, *14*, 304. [CrossRef]

49. Hideo, N.; Ryuichi, I.; Yosuke, H.; Hiroyuki, S. Effects of surface roughness on wettability. *Acta Mater.* **1998**, *46*, 2313–2318. [CrossRef]

50. Żenkiewicz, M. *Adhezja i Modyfikowanie Warstwy Wierzchniej Tworzyw Wielkocząsteczkowych*; Wydawnictwo Naukowo-Techniczne: Warszawa, Polska, 2000; pp. 81–83.

51. Kubiak, K.J.; Wilson, M.C.T.; Mathia, T.G.; Carval, P. Wettability versus roughness of engineering surfaces. *Wear* **2011**, *271*, 523–528. [CrossRef]

52. Candan, Z.; Büyüksarı, U.; Korkut, S.; Unsal, O.; Çakıcıer, N. Wettability and Surface Roughness of Thermally Modified Plywood Panels. *Ind. Crops Prod.* **2012**, *36*, 434–436. [CrossRef]

53. Papp, E.; Csiha, C. Contact angle as function of surface roughness of different wood species. *Surf. Interfaces* **2017**, *8*, 54–59. [CrossRef]

54. Yorur, H.; Erer, A.M.; Oğuz, S. Effect of surface roughness on wettability of adhesive on wood substrates. In Proceedings of the 3rd International Conference on Science, Ecology and Technology, Rome, Italy, 14–16 August 2017.

55. Yuningsih, I.; Rahayu, I.S.; Lumongga, D.; Darmawan, W. Wettability and adherence of acrylic paints on long and short rotation teaks. *Wood Mater. Sci. Eng.* **2019**, *15*, 229–236. [CrossRef]

56. Bartoszuk, K.; Kowaluk, G. The Influence of the Content of Recycled Natural Leather Residue Particles on the Properties of High-Density Fiberboards. *Materials* **2023**, *16*, 5340. [CrossRef]

57. Yu, Q.; Pan, X.; Yang, Z.; Zhang, L.; Cao, J. Effects of the Surface Roughness of Six Wood Species for Furniture Production on the Wettability and Bonding Quality of Coating. *Forests* **2023**, *14*, 996. [CrossRef]

58. Casilla, R.C.; Chow, S.; Steiner, P.R. An immersion technique for studying wood wettability. *Wood Sci. Technol.* **1981**, *15*, 31–43. [CrossRef]

59. Wang, X.F.; Wei, X.F.; Huang, P.Q. Study on Performance of Adherence of Water-Base UV Varnish. *Adv. Mater. Res.* **2010**, *174*, 409–412. [CrossRef]